Journal of Materials Chemistry A

ROYAL SOCIETY OF CHEMISTRY

PAPER

View Article Online
View Journal

Cite this: DOI: 10.1039/d6ta00751a

In vacuo XPS study: controlled ALD growth of Al_2O_3 on metallic lithium enabled by plasma pretreatment

Tippi Verhelle, [a] Lowie Henderick, [a] Saeed Yari,[bcd] Siebe Coessens, [a] Matthias M. Minjauw,[a] Louis De Taeye, [ce] Philippe M. Vereecken,[ce] Jolien Dendooven, [a] Mohammadhosein Safari [bcd] and Christophe Detavernier*[a]

Direct atomic layer deposition (ALD) of protective coatings on metallic lithium is a promising strategy to suppress unwanted side reactions in next-generation batteries. Although several studies report ALD coatings on lithium, with the majority depositing Al_2O_3, inconsistencies in growth behavior are present. Also in this work, the deposition of Al_2O_3 using trimethylaluminium (TMA) and O_2 plasma on as-received metallic lithium results in irreproducible and non-ALD-like growth. This highlights the need for a fundamental understanding of how the initial surface state governs subsequent ALD reactions. In this work, plasma pretreatments are used to systematically control the lithium surface and *in vacuo* X-ray photoelectron spectroscopy (XPS) is used during the TMA/O_2 plasma ALD process in order to understand its growth behavior on metallic lithium. The as-received lithium surface consists of Li_2CO_3, LiOH and Li_2O, with composition evolving over time, making it an unreliable starting surface for ALD. Argon plasma pretreatment efficiently removes carbon contamination, producing a Li_2O-terminated surface, while O_2 plasma results in a mixed LiOH/Li_2O surface. Self-limiting, ALD-like growth of (lithiated) Al_2O_3 is observed only on the LiOH/Li_2O surface, enabled by reactive hydroxyl groups that facilitate TMA adsorption. In contrast, TMA exposure on the Li_2O surface results in immediate precursor decomposition, likely due to a porous nature of the Li_2O layer allowing direct interaction between TMA and the bulk lithium underneath. These results show that controlling and clearly defining the initial surface state is essential for achieving reproducible ALD growth on metallic lithium and may help explain the inconsistencies reported in earlier studies.

Received 26th January 2026
Accepted 17th April 2026

DOI: 10.1039/d6ta00751a

rsc.li/materials-a

1 Introduction

The sustainable electrification of our society is more than ever at the center of global discussions. Lithium-ion batteries (LIBs) can play an essential role in enabling this transition. Due to their high energy density and long cycle life, they are widely being used for energy storage in electrical vehicles and large-scale energy storage systems.[1] However, as demand for increasing performance continues to grow, state-of-the-art LIBs are approaching their energy density limits, driving the search for next-generation battery chemistries.[2] Metallic lithium has long been considered as the 'holy grail' of anode materials due to its high theoretical specific capacity (3860 mA h g^{-1}) and low electrochemical potential (−3.04 V *vs.* standard hydrogen electrode).[1] Combining metallic lithium with current or next-generation cathode materials could result in higher energy density batteries.[2] Although promising in theory, the practical implementation of lithium metal anodes remains a significant challenge.

Upon contact with the electrolyte, a solid-electrolyte interphase (SEI) is formed on the lithium metal surface due to electrolyte reduction. The SEI continues to grow during cycling, leading to progressive loss of active lithium.[2] Due to the SEI's complex and inhomogeneous composition,[2–6] properties such as ionic conductivity are also non-uniform across the surface, resulting in preferential ion transport through pathways of least resistance.[4,7] As a result, lithium-ion deposition happens at localized 'hot spots',[5,8] initializing the formation of dendritic structures.[5,8,9] Once nucleated, these dendrites grow in size and shape and induce stress upon the SEI, resulting in fractures and exposure of fresh lithium, thereby triggering additional parasitic reactions and repeated SEI formation.[4,6,7,10] During discharge, dendrites are not completely stripped due to the thick and uneven SEI,[4] resulting in electrically isolated lithium,

[a]*Department of Solid State Sciences, Ghent University, Krijgslaan 285 S1, 9000 Gent, Belgium. E-mail: Christophe.Detavernier@Ugent.be*
[b]*Institute for Materials Research (IMO-imomec), UHasselt, Martelarenlaan 42, 3500, Hasselt, Belgium*
[c]*Energyville, Thor Park 8320, 3600, Genk, Belgium*
[d]*Imec Division IMOMEC, 3590, Diepenbeek, Belgium*
[e]*Imec, Kapeldreef 75, Leuven, 3001, Belgium*

referred to as dead lithium.[4,6,10] Clearly, this behavior of continuous loss of electrolyte and lithium severely degrades the performance of the lithium metal battery. In severe cases, dendrites can grow into needle-like structures capable of piercing the separator, posing a serious risk for short-circuits and thermal runaway.[2,6,7]

This problem highlights the critical role of the inhomogeneity of the SEI's composition in the battery performance.[9] To address this issue, different strategies aim to passivate the lithium surface with a homogeneous and stable artificial SEI layer with uniform interfacial properties to improve cycle lifetime and safety of the lithium metal battery.[2,5,6] One approach is solution-based and involves engineering the liquid electrolyte by modifying salts, solvents or adding additives. Although a protective SEI can be formed, the resulting SEI composition is dictated by uncontrolled decomposition products.[6] Vacuum techniques such as magnetron sputtering and atomic layer deposition (ALD), offer more control over composition and thickness.[6] ALD, which relies on self-limiting surface reactions by sequentially introducing individual precursor gases, enables the growth of conformal coatings with precise atomic-scale thickness control.

In 2015, Kozen *et al.*[11] demonstrated the direct deposition of Al_2O_3 on Li metal foil using TMA and O_2 plasma, reporting that a 14 nm film could delay atmospheric and organic solvent corrosion, leading to an overall improved discharge capacity retention in Li–S batteries. Shortly thereafter, Kazyak *et al.*[12] showed that even a limited number of ALD cycles (*e.g.* 30 cycles of TMA–H_2O) could already significantly extend the cycle lifetime and suppress dendrite formation. While these pioneering studies highlighted the potential of ALD coatings for Li metal protection, growth mechanisms were not studied. Thickness was reported on a conventional Si wafer,[11] however, TMA or H_2O do not necessarily react in self-limiting ways with the Li surface. The importance of differentiating between layer growth on silicon *versus* lithium was highlighted by Chen *et al.*[13] They reported that the initial TMA and H_2O reactions on Li do not saturate, leading to more deposited material than expected, when compared to growth on Si. Although promising results could be obtained, with the abovementioned contributions forming a promising starting point for optimized lithium surfaces, general progress has been slow with only few studies further exploring ALD on Li metal.[14–23] Furthermore, it is often not specified whether the used lithium foil has undergone any pretreatment step before ALD. Some mention using the lithium foil as-received, while others mechanically scraped the foil.[22] As-received lithium foil contains a native surface layer, with contaminants such as Li_2CO_3, LiOH and Li_2O,[15,24,25] even under inert storage, with composition evolving over time. Previous results highlight that ALD surface enhancement for metallic lithium could be very promising, but more effort is needed in order to fully understand how native surface species interact with ALD precursors, such as TMA, and how further ALD growth is influenced.

In this work, we address this knowledge gap by studying the initial interaction between TMA and plasma pretreated lithium surfaces. Instead of starting from as-received foil, the lithium surface composition is tailored through Ar and O_2 plasma pretreatments performed in the same high vacuum (HV) chamber as the subsequent ALD process. These plasma pretreatments (partially) remove the native surface layer and produce a defined and reproducible starting surface in a more controlled manner. For comparison, the reaction of TMA on as-received and mechanically treated lithium foils is also investigated. Scanning electron microscopy (SEM) reveals that highly non-reproducible and localized growth is obtained for the as-received and mechanically treated foil. *In vacuo* X-ray photoelectron spectroscopy (XPS) and SEM results indicate that Ar plasma pretreatment promotes TMA decomposition, while after an O_2 plasma pretreatment step, controlled deposition of (lithiated) Al_2O_3 is possible. These findings demonstrate that precursor reactivity and growth evolution depend on the initial lithium surface. Establishing a controlled and reproducible starting surface is therefore essential for understanding and controlling ALD processes on Li foil.

2 Experimental section

A custom-built cluster tool, schematically shown in Fig. 1, was used for *in vacuo* XPS characterization. This system includes a pump-type ALD reactor (base pressure: 10^{-7} mbar) directly connected to a Theta Probe XPS (base pressure: 10^{-9} mbar). An Ar-filled glovebox (H_2O/O_2 < 0.5 ppm) is integrated into this system and is connected to the ALD reactor through an UHV transfer line (10^{-9} mbar), allowing sample handling in an inert environment. Lithium samples (250 μm, Cambridge Energy Solutions Ltd) are treated in the ALD setup and then transferred to the XPS chamber in vacuum (10^{-7} mbar) and in under two minutes, minimizing contamination risk. For each XPS measurement, a fresh piece of lithium foil was treated and analyzed, avoiding repeated transfers and further reducing the risk of contamination. Each piece was separately loaded into the reactor where the full pretreatment and ALD sequence was performed and stopped at the step of interest. To ensure reproducibility and account for foil-to-foil variability, selected measurements were repeated up to three times, each on a new piece of lithium foil.

Plasma pretreatments were conducted in the ALD reactor, which was equipped with a plasma column (diameter: 63 mm) on top, above the substrate, ensuring line-of-sight, without substrate bias. Plasmas of Ar (≥99.999%) and O_2 (99.5%) were generated by a remote inductively coupled plasma source of 13.56 MHz operated at 200 W, with each gas maintained at a pressure of 1×10^{-3} mbar. The influence of plasma pressure is elucidated in the SI, Fig. S1, showing the importance of maintaining a low pressure to ensure surface etching. Subsequent ALD treatments involved trimethylaluminium (TMA, $Al(CH_3)_3$, 97%, Volatec, 10^{-2} mbar) in combination with O_2 plasma (200 W, 5×10^{-3} mbar), with the first TMA dose pulsed immediately after the plasma pretreatment, with only 15 s of pumping in between. The ALD cycle consisted of a 60 s TMA pulse, 30 s pumping, 30 s O_2 plasma exposure and 30 s pumping. Substrate temperature during treatments was maintained at 100 °C, unless mentioned otherwise.

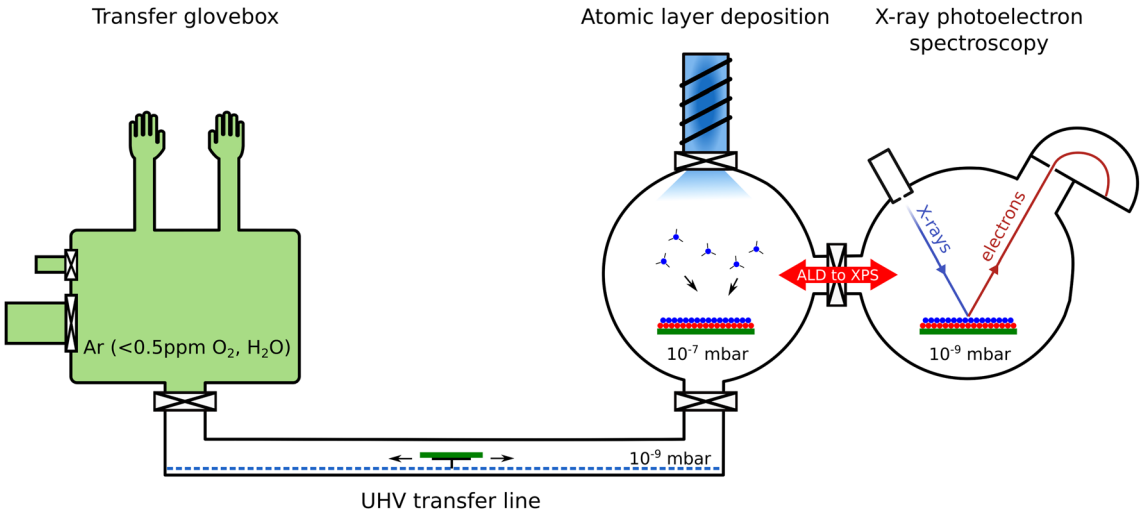

Fig. 1 Illustration of the glovebox-ALD-XPS cluster tool used in this work.

XPS measurements were performed using a Theta Probe XPS system with a monochromatic Al Kα source (15 kV, 70 W) focused to a 0.3 mm diameter spot and incident at 30° relative to the surface normal. The concentric hemispherical analyzer accepted electrons over a wide angular range (20°–80° relative to the surface normal) and the input lens was positioned at 50°. High-resolution spectra were acquired using a pass energy of 50 eV and a step size of 0.1 eV, while survey spectra were collected at 200 eV pass energy and 0.5 eV step size. Charge neutralization was not used. Quantification and peak fitting were carried out using CasaXPS,[26] employing a U 2 Tougaard background and LA(50) line shapes. Binding energy referencing could not be performed based on the adventitious hydrocarbon C 1s core level as the C 1s signal was not always present, hence the O 1s Li_2O peak was used and positioned at 531.2 eV.[27] A minor Li_2CO_3 contribution in the C 1s signal, when present, served as additional consistency check. Reference samples of Al_2O_3 were also prepared on Si substrates to provide an internal reference for the Al_2O_3 O 1s peak. Peak fitting of Li_2CO_3, LiOH and Li_2O was done based on binding energy separations determined in the work of Wood *et al.*[27] and were constrained within narrow intervals. The O 1s FWHM values were kept consistent across spectra.

Surface morphology was characterized using scanning electron microscopy (JEOL JSM-IT800, accelerating voltage of 10 kV) with a secondary-electron detector. Elemental analysis was performed by energy-dispersive X-ray spectroscopy (EDX, OXFORD X4 Xplore 30) at a working distance of 10 mm. Treated lithium foils were transferred to the SEM without air exposure, making use of the Environmental Cell Specimen Holder.[28]

3 Results and discussion

3.1 Starting surface

A pretreatment step is often not mentioned in other work, implying that the lithium foil is used as-received. It is well-known that commercial lithium foil develops a native surface layer during manufacturing and glovebox storage,[15,24,25] which we also observe in our *in vacuo* XPS measurements, shown in Fig. 2(a). The C 1s spectrum shows a dominant Li_2CO_3 peak at 293 eV, along with adventitious carbon at 288.2 eV, shifted from the common 285 eV due to charging, as reported by Wood *et al.*[27] The Li_2CO_3 signal is also visible in the Li 1s (at 58.1 eV) and in the O 1s (at 534.8 eV) spectra. An additional peak at 56.2 eV for Li 1s and 531.2 for O 1s is present, corresponding to Li_2O.[27] A minor feature around 55 eV in the Li 1s region indicates the presence of Li^0, suggesting that the native layer is either sufficiently thin or locally discontinuous to allow detection of the underlying lithium metal. SEM imaging of this surface, Fig. 2(b), shows a relatively smooth morphology. However, the composition of the native layer is highly dependent on how the lithium foil has been manufactured and on storage time in the glovebox.[25] Depending on how the foil was prepassivated, other contaminants, such as P and F, could also play a role.[29] Furthermore, by leaving the foil inside the glovebox for a couple of weeks, the fraction of carbonate at the surface increases and generally, a thicker native layer is obtained.[25] This makes the comparison between different studies more difficult, as often the state of the initial surface is not reported[7] and it is unclear how this influences ALD growth. To make sure that depositions are always performed in the same manner, a pretreatment step, resulting in a reproducible surface, should be applied.

A common pretreatment is mechanical treatment, *i.e.* scraping the foil to remove the native layer, creating a more reactive lithium surface. While straightforward, this approach is time sensitive since the scraping can only be performed in the glovebox, where the freshly exposed surface reacts with residual gases, meaning its state at deposition strongly depends on the delay between scraping and transfer.

To gain better control over the surface composition, we carried out a plasma pretreatment step in the same vacuum chamber as the deposition. Similar plasma treatments have been used in our previous work[30] to generate distinct surface chemistries. In this work, we solely focus on Ar and O_2 plasma, from now on denoted as Ar* and O_2^*. Ar* treatment, shown in

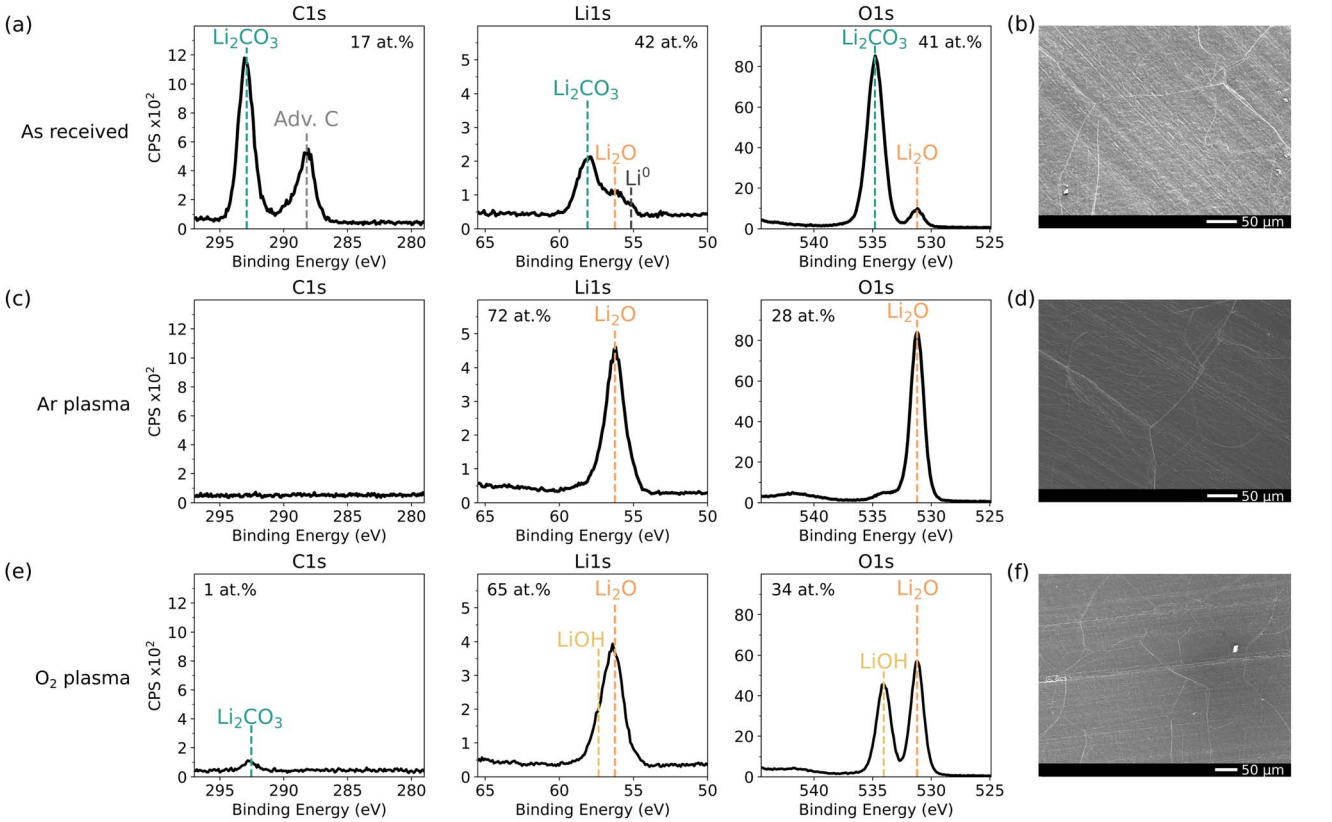

Fig. 2 *In vacuo* XPS spectra of C 1s, Li 1s and O 1s and SEM images of (a and b) as-received, (c and d) Ar* and, (e and f) O_2^* treated lithium foil. Survey spectra can be found in Fig. S2.

Fig. 2(c), fully removes carbon contamination and produces a Li_2O surface, as observed in the Li 1s and O 1s spectra. From our own experience and reported in literature,[24,27,31] obtaining a pure metallic Li surface by ion bombardment remains challenging. This can be attributed to the extreme reactivity of Li, which readily forms Li_2O *via* trace H_2O from the reactor or Ar gas impurities. Even in UHV, continuous sputtering is needed to sustain the metallic nature.[27] Furthermore, Li_2CO_3 decomposes into Li_2O under ion bombardment, releasing CO_2 gas:[24,27]

$$Li_2CO_3 \rightarrow Li_2O + CO_2(g)$$

In practice, both mechanisms likely contribute to the Li_2O surface. O_2^* treatment (Fig. 2(e)) similarly removes most carbon contamination, although a small amount of C (1 at%) in the form of Li_2CO_3 remains, potentially due to incomplete etching or CO_2 redeposition.[32,33] In addition to Li_2O, the O 1s spectrum shows an additional component at 534 eV, which we attribute to LiOH. Distinguishing LiOH from Li_2O_2 is difficult due to overlapping binding energies and identical Li : O ratios, as noted by Wood *et al.*[27] This feature likely also arises from residual background species interacting with the plasma or incomplete etching. Both plasma treatments maintain a smooth surface morphology observed by SEM (Fig. 2(d and f)).

To obtain additional information on layer thicknesses, angle-resolved XPS (ARXPS) measurements were performed on the as-received, Ar* and O_2^* pretreated surfaces (Fig. S3). ARXPS was preferred over sputter depth profiling, as ion bombardment can significantly alter the surface chemistry.[25,27] For as-received lithium, the Li^0 and Li_2O signals decrease with increasing surface sensitivity, confirming that these species are located beneath the Li_2CO_3 layer, consistent with previous reports.[25] For both Ar* and O_2^* treated lithium, a weak Li^0 signal remains detectable at low emission angles, indicating that metallic lithium is still accessible beneath the oxide/hydroxide layers, which are therefore relatively thin (within the XPS probing depth of $\sim$ 5–10 nm). Furthermore, ARXPS shows that the LiOH contribution becomes more pronounced at higher emission angles, indicating LiOH-enrichment near the outermost surface.

3.2 TMA exposure on as-received metallic lithium

Although several reports on ALD of Al_2O_3 on as-received lithium exist,[11,13,15,19,20,23] the initial TMA exposure and further ALD growth has not been discussed in much detail. In this work, we exposed as-received lithium foils to different cycles of TMA-O_2^*, with a TMA pulse of 60 s and O_2^* exposure of 30 s. Each of these foils were then investigated with SEM.

After exposing a lithium foil to 60 s of TMA, isolated black spots were visible on the foil. SEM imaging of these black spots, Fig. 3(a and b) showed that these were dispersed particles, already a few micrometers in size, mainly nucleating around the

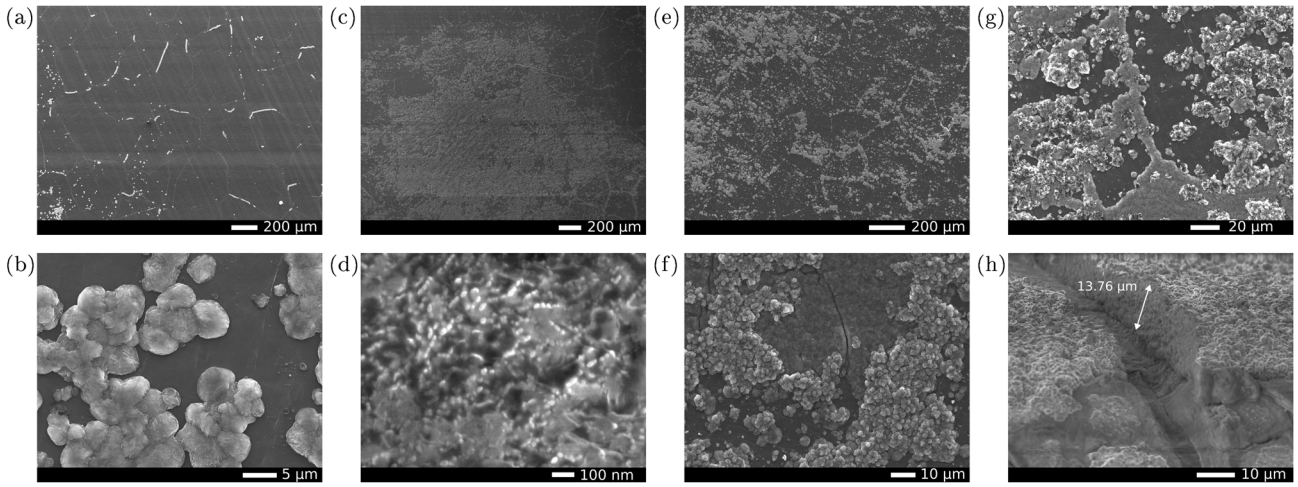

Fig. 3 SEM images of (a and b) lithium foil without any pretreatment after a 60 s TMA pulse, (c and d) after 5 cycles TMA – O_2^*, (e and f) after 10 cycles and (g and h) after 100 cycles.

grain boundaries. EDX measurements on these particles, exhibited a strong Al signal compared to the surrounding smooth surface where little to no Al was detected (Fig. S4), indicating extensive reactions between TMA and the surface, unlike conventional ALD growth on a Si wafer.

With more ALD cycles, the density of the black regions increased and SEM images (Fig. 3(c–f)) show that the structures are merging together. The deposited material appeared porous, consisting of densely packed pillar-like structures. After 100 cycles, the foil was completely covered in black spots and SEM (Fig. 3(g and h)) shows an exceptionally thick layer of ~10 µm, far exceeding the 15–20 nm typically obtained on Si under similar ALD conditions.

Notably, this outcome was not consistently reproducible. With identical process conditions and the same batch of as-received lithium foil, the foil sometimes remained metallic without black spots, with only very sparse particles visible in SEM. We believe that the way the initial TMA reaction happens, strongly dictates the subsequent growth mode. When extensive nucleation occurs in the first cycle, growth proceeds more uncontrolled, whereas fewer nucleation sites may result in a more ALD-like growth. Furthermore, this is in contrast with the results reported by Kang *et al.*,[20,23] where they demonstrated that longer TMA pulses (5–30 s) result in blackening of the foil due to the formation of a Li–Al–C layer, several micrometers thick after only 20 s of TMA exposure. The reason for this inconsistent behavior remains unclear, but it could be related to variation in the morphology, microstructure (*e.g.* increased presence of defects at grain boundaries[4,15]) and thickness of the native surface layer and/or the sample surface history (*i.e.* the contaminant exposure accumulation since production), which highlights the importance of controlling the starting surface.

3.3 TMA exposure on an Ar plasma pretreated lithium surface

In order to obtain consistent results, the surface should be as reproducible as possible. This can be achieved through a pretreatment step, such as mechanical scraping of the lithium foil or plasma pretreatments.

Even though mechanical scraping is an effective technique to remove the native layer, the freshly exposed surface is rapidly recontaminated. As an example, we scratched the top half of a piece of Li foil and left it in the glovebox for 10 minutes before scratching the other half. The foil was then transferred to the ALD reactor in under one minute and exposed to 30 s of TMA. Fig. 4(a) illustrates the effect of recontamination as the freshly scratched half turned completely black, whereas the 'aged' half remained relatively shiny. Since this surface cannot be controlled in a reproducible manner, mechanical scraping as a pretreatment will not be further discussed.

In order to limit the risk of recontamination, pretreatment steps should be performed in the same vacuum chamber as the ALD process. In this work, we use plasma treatments inside the ALD reactor to ensure reproducible starting surfaces. For the Li_2O starting surface, obtained after Ar* treatment, a 30 s TMA exposure leads to a similar outcome as the scratched foil, rapidly coloring the surface visibly black (Fig. 4(b)), again pointing at substantial reactions between TMA and lithium. SEM imaging after just 2 s of TMA shows pronounced morphological changes (Fig. 4(c)). The surface is densely covered with spherical particles, with growth into pillar-like structures occurring simultaneously at certain places. This morphology is similar to TMA exposure on as-received lithium foil, however, in this case, the particles appear more rapidly and they are smaller and more densely packed. Already from 5 s of TMA, the surface appears completely black and Fig. 4(d and e) shows that the surface is completely covered with these pillars, however, forming a porous morphology visible from the voids in between. Extended exposure of TMA results in continuous growth as a cross-sectional SEM image after 30 s TMA shows a thickness of ~2 µm Fig. 4(f and g).

XPS analysis of Ar* treated lithium exposed to 30 s of TMA at a substrate temperature of 100 °C, reveals significant incorporation of Al (18 at%) and C (46 at%), with only a small amount of oxygen. High-resolution scans are shown in Fig. 5 for different

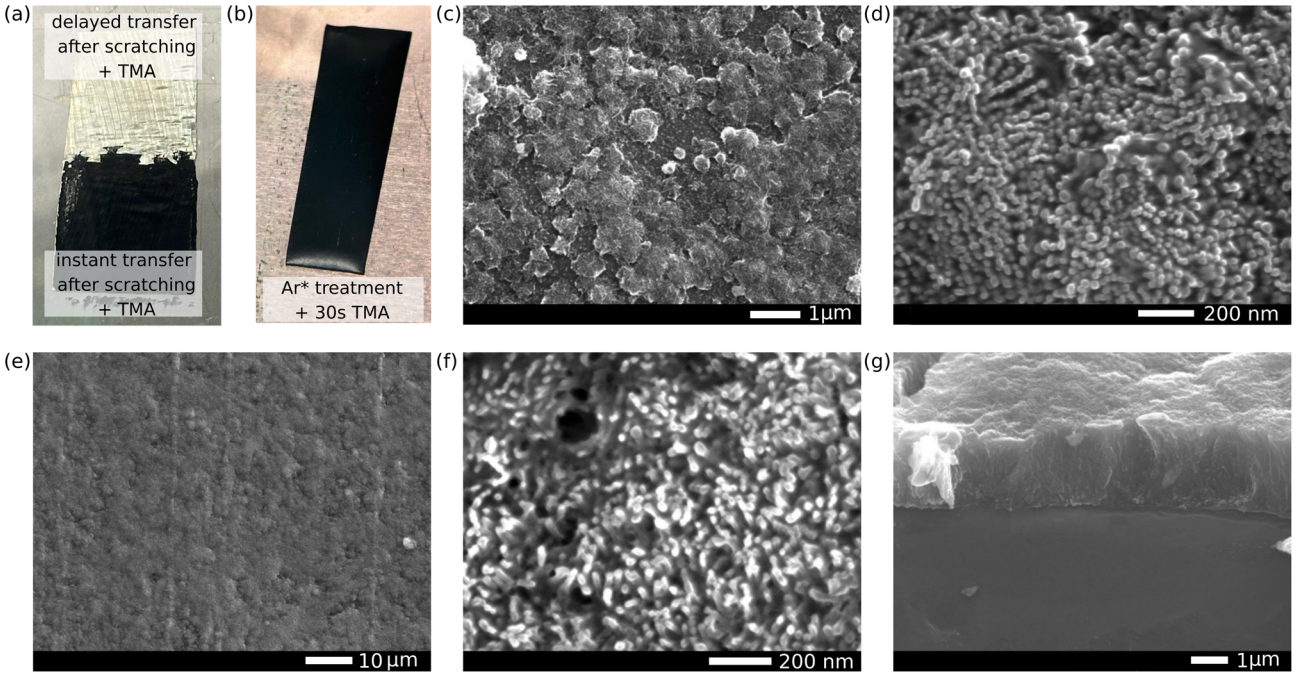

Fig. 4 Visual image of a blackened foil after 30 s of TMA exposure (a) after scraping the foil with rapid transfer (bottom part) and 10 min storage in glovebox (top part) and (b) after 30 s of TMA exposure after Ar* treatment. SEM image of (c) 2 s, (d and e) 5 s and (f) 30 s of TMA exposure on a Li_2O surface after Ar* treatment with (g) a cross-sectional image.

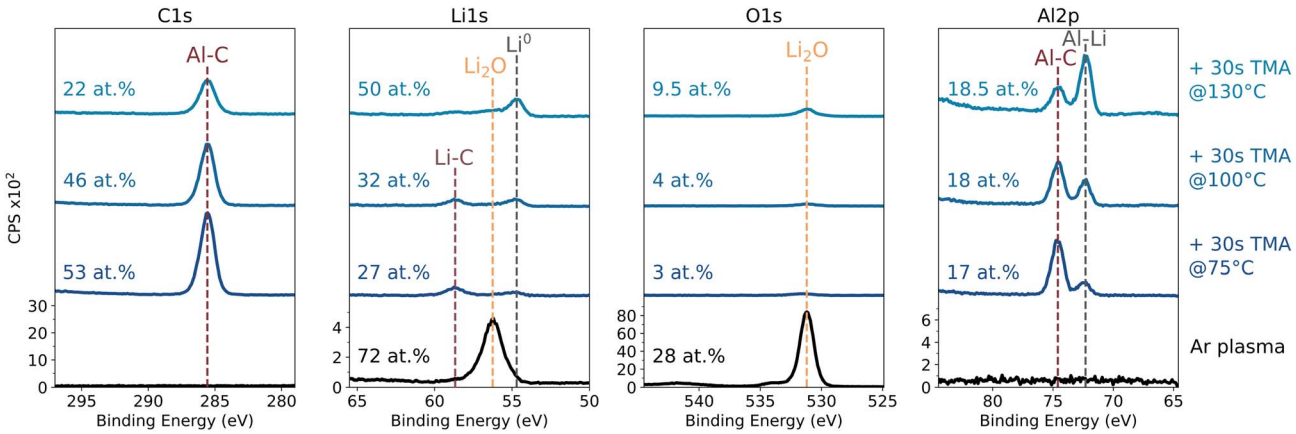

Fig. 5 *In vacuo* XPS of an Ar* treated Li foil exposed to a 30 s dose of TMA at temperatures of 75, 100 and 130 °C. Survey spectra are available in Fig. S5.

substrate temperatures. The Al 2p spectrum shows two distinct peaks, at 74.6 eV and 72.4 eV. Given the low O content, an Al–O bond is less likely and is found in our case at higher binding energies (*i.e.* 76.6 eV,[34,35] see discussion below). Both the Al 2p component at 74.6 eV and the C 1s peak at 285.6 eV decrease proportionally in signal intensity with increasing substrate temperature, maintaining a constant C/Al atomic ratio of ~3.7. This correlated behavior indicates that these signals are chemically linked and therefore, we have labeled these peaks as Al–C, even though an exact match in literature was not found.[35] In parallel, the Al 2p peak at 72.4 eV, which is close to the expected metallic Al binding energy,[35] increases in intensity with increasing substrate temperature. A similar trend is observed for the Li 1s signal at 54.8 eV, which corresponds to metallic Li.[27] Furthermore, a small peak is visible around 58.7 eV, which we have tentatively assigned to Li–C bond. These results indicate that TMA exposure leads to an Al–C rich surface at lower temperatures, gradually shifting towards a more metallic character with increasing substrate temperature. The reason for this is unclear, but it could be related to more mobile Li atoms at higher temperatures as the substrate temperature is nearing the lithium melting point of 180 °C.

At a substrate temperature of 100 °C, the surface composition consisted out of 46 at% C, 32 at% Li, 18 at% Al and 4 at% O,

which appears similar to the Li–Al–C layer reported by Kang *et al.*,[20,23] with a composition of 30 at% C, 40 at% Li, 20 at% Al and 10 at% O, as determined by XPS.

While XPS provides surface sensitive information (5–10 nm), SEM reveals that the layer quickly grows into the micrometer range. In order to get an idea about the bulk composition, an EDX linescan was performed across a cross-sectional SEM image. Fig. S6 shows that while the outer surface is indeed C-rich, the C content in the bulk decreases. In contrast, the Al signal also decreases with depth, but remains substantial throughout the cross-section, indicating significant Al incorporation beyond the surface layer, likely pointing to a more Al–Li character.

The above results indicate that after an Ar* pretreatment, TMA decomposes onto the surface and conventional ALD growth cannot be obtained. A straightforward chemical pathway between TMA and Li_2O that could support continuous growth is not easily thought of. The O^{2-} anions in Li_2O are strongly bound to Li^+ and lack available protons for ligand exchange, making direct reaction with TMA unfavorable. We therefore hypothesize that the Li_2O surface layer contains defects or voids that allow interaction with the underlying metallic lithium, an interpretation that is consistent with its low Pilling-Bedworth ratio (PBR)[36] of 0.57. A PBR below unity indicates that the oxide is unlikely to fully passivate the metal surface, as molar volume mismatch between the metal and the oxide induces cracks or voids, exposing the metallic lithium underneath.[25,36,37] Such exposed Li can act as a powerful reducing agent capable of donating electrons to the TMA precursor and thereby promoting reductive decomposition and potentially transmetalation of the methyl-ligands to form Li–C species. Concurrent formation and diffusion of elemental Al into the bulk can lead to Li–Al alloying, explaining the continuous growth and uncontrolled film formation.[23] Even though the exact decomposition mechanism is not fully understood, our results suggest that access to metallic Li beneath the Li_2O layer likely plays a dominant role in the observed film growth. Detailed calculation and interpretation of the PBR is incorporated in the SI.

3.4 TMA exposure on an O_2 plasma pretreated lithium surface

If the uncontrolled reactivity originates from exposed metallic lithium beneath a defective or non-passivating Li_2O layer, then forming a more passivating surface layer should suppress direct electron transfer and enable self-limiting ALD surface reactions. O_2^* plasma pretreatment was therefore explored, as it produces not only Li_2O, but also a LiOH component, as shown in Fig. 2. LiOH has a PBR value of 1.26 (SI), which is above unity and therefore consistent with formation of a continuous, passivating layer.

In contrast to the Ar* pretreatment, the surface of an O_2^* treated lithium foil exposed to TMA remained visually metallic, no black spots were visible, even after 120 s of TMA exposure (Fig. 6(a)). With SEM, a smooth surface remained (Fig. 6(b)) and a low Al signal was measured with EDX.

From *in vacuo* XPS measurements, we were able to determine the saturation behavior of TMA and O_2^* during the first ALD cycle. Fig. 6(c) and S7 show that saturated ALD-like growth is observed for TMA after 60 s of exposure. The data points in Fig. 6(c) were obtained from the peak areas of high-resolution Al 2p scans in Fig. S7. The Al 2p peak after 60 s is relatively small,

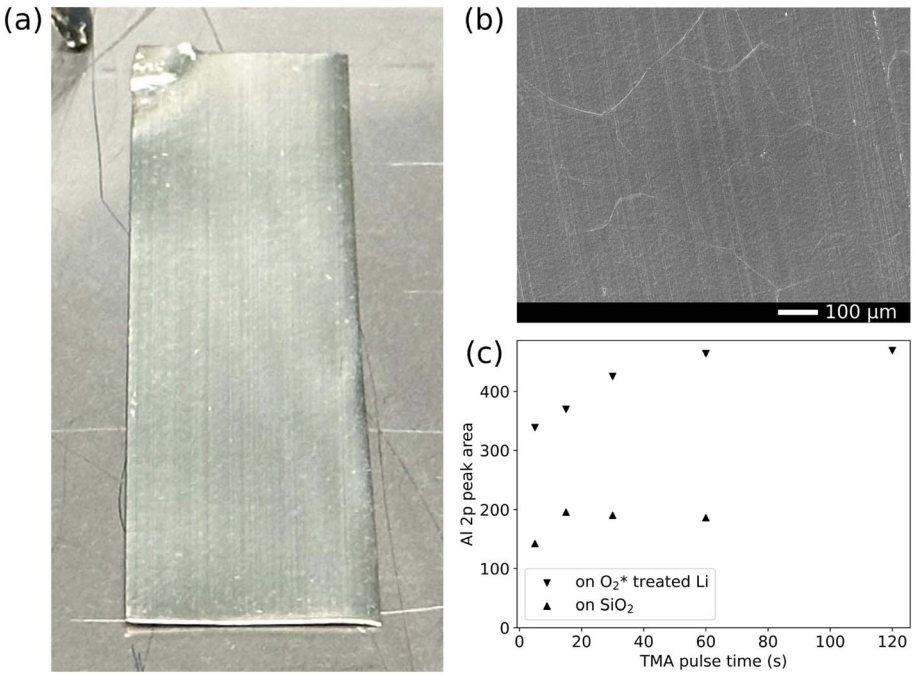

Fig. 6 O_2^* treated lithium foil exposed to 120 s of TMA (a) visual image and (b) SEM image, with (c) the TMA saturation behavior on O_2^* treated Li *versus* on the SiO_2 surface of a Si wafer as determined by XPS.

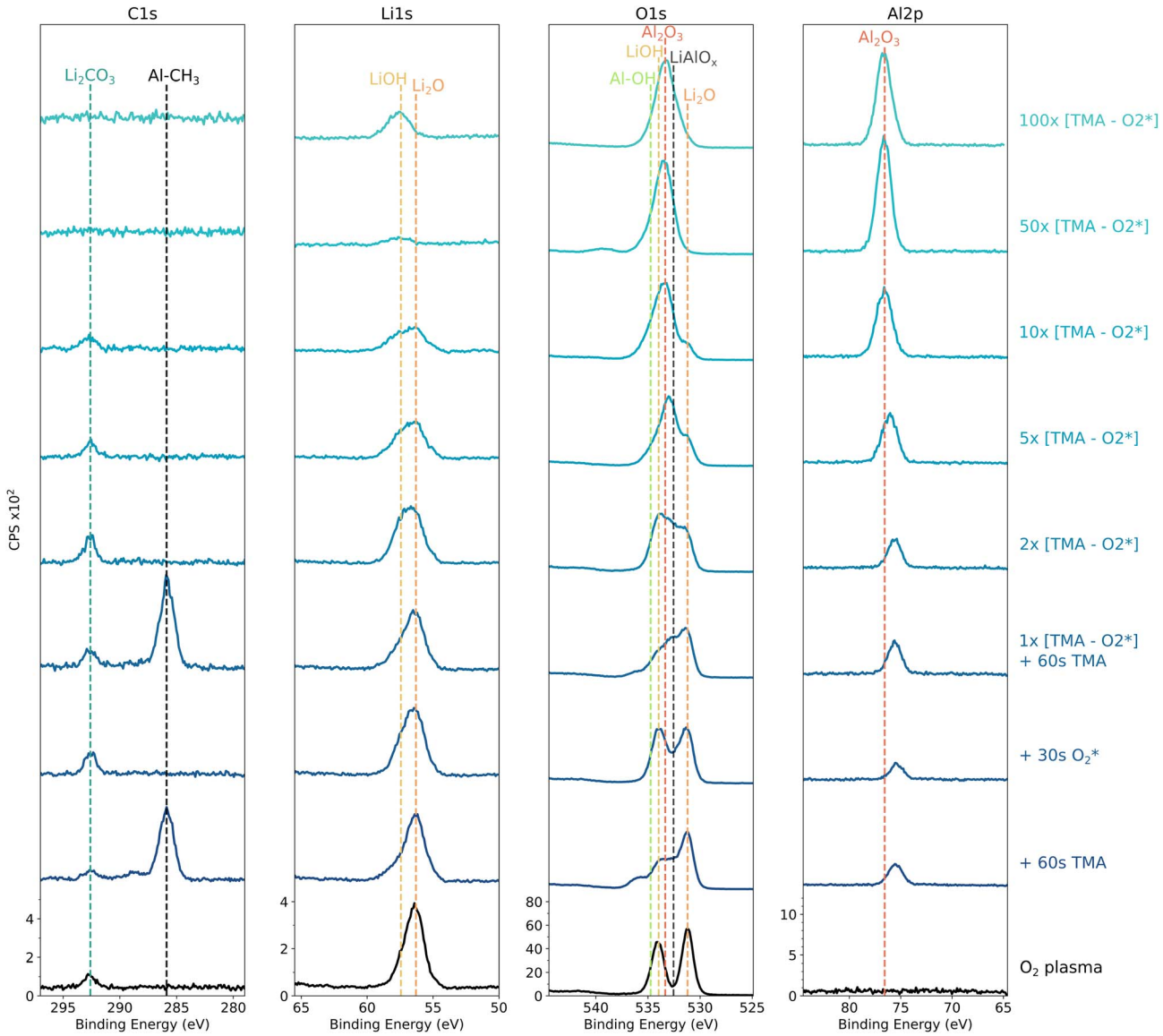

Fig. 7 *In vacuo* XPS of O_2^* treated Li after a different number of ALD cycles of TMA – O_2^*. *Y*-axes were kept the same to show real intensity differences. Survey spectra and atomic percentages can be found in Fig. S8 and Table S1.

well below the maximum intensity expected from the photoelectron information depth, as shown in Fig. 7, indicating that the observed saturation arises from self-limiting surface reactions rather than signal attenuation due to layer thickness. Although saturating, the measured Al 2p peak area for TMA exposure on Li is higher than that on Si, suggesting more Al material is incorporated after a single pulse and hinting at a non-conventional reaction mechanism.

After exposing the O_2^* plasma treated lithium to 60 s of TMA, the LiOH (534 eV) and Li_2O (531.2 eV) components in the O 1s spectrum decrease in intensity, indicating partial consumption of the surface –OH groups by TMA (Fig. 7). Expected from this reaction is an Al–CH_3 terminated surface,[34] which is confirmed by the presence of an Al 2p peak at 75.5 eV and the C 1s peak at 285.9 eV. Furthermore, a third peak appears in the O 1s spectrum at $\sim$ 532.6 eV, likely due to Al–O bonds that have formed on the surface. However, the binding energy does not exactly correspond with reported Al_2O_3 binding energy values.[34,38] The O 1s component at 532.6 eV is therefore more likely related to an $LiAlO_x$ layer, which has been suggested by others,[13,19,22] as it is found at lower binding energies than Al_2O_3, however, without consistent peak labeling through the different reports. A small shoulder is observed in the O 1s spectrum at higher binding energies (536 eV) and is further discussed in Fig. S8. The initial reaction between TMA and the O_2^* pretreated surface was also investigated at substrate temperatures of 75 and 130 °C. However, no significant differences in spectra were observed and therefore, the substrate temperature was kept at 100 °C to study further growth.

To complete the first ALD cycle, the surface was exposed to O_2^*. High-resolution XPS scans in Fig. S7 show that O_2^* saturation is reached after 30 s for all spectra. Therefore, saturated

conditions of 60 s TMA and 30 s O_2^* are used for further depositions. After the 30 s O_2^* exposure, an increase in LiOH O 1s signal is observed, also clear from broadening of the Li 1s peak due to the LiOH component at 57.4 eV, as shown in Fig. 7. Furthermore, O_2^* efficiently removes the methyl ligands through combustion, however, a small amount of Li_2CO_3 is detected, probably from limited CO_2 redeposition.[32,33]

After the second cycle, the Li_2O signal further decreases while the LiOH intensity remains nearly unchanged, indicating that either the lithium is able to diffuse through the thin surface layer to interact with the energetic plasma or that the thin layer is not yet continuous. After 5–10 cycles, these components become smaller. Furthermore, the Al 2p peak progressively shifts to higher binding energies, eventually remaining at the peak position of 76.6 eV after 10 cycles. A similar evolution is observed for the O 1s spectra, where the main peak shifts to 533.4 eV. The binding energy difference between these Al 2p and O 1s components (456.8 eV) closely matches reported values for Al_2O_3,[34,38] confirming the formation of an Al_2O_3 surface layer and confirming that the initial O 1s peak at 532.6 eV could be related to $LiAlO_x$.

Although the Li 1s signal decreases with increasing ALD cycle, the signal reappears after 100 cycles, implying that lithium is able to diffuse through relatively thick Al_2O_3 films over extended timescales. Another reason could be due to cracking of the layer or pinhole formation, however, this was not obvious from SEM images (Fig. S9). Compared to 50 cycles, the O 1s peak broadens, suggesting a mixture of lithiated and non-lithiated Al_2O_3. Even though Kozen *et al.*[11] reported no Li 1s signal after '14 nm' of Al_2O_3, more recent work shows a clear lithium signal for more than 100 ALD cycles.[19,22]

From these XPS results, it is clear that a (lithiated) Al_2O_3 thin film can be grown in a much more controlled way when O_2 plasma is used for pretreatment. SEM imaging (Fig. S9) shows that after 50 and 100 cycles of TMA-O_2^*, the surface remains smooth and without change in morphology. Furthermore, EDX measurements confirm that the Al signal is comparable to what is expected on Si (Fig. S10). Even though more material is getting incorporated in the initial cycle, this excess uptake is hypothesized to be associated with the formation of a thin $LiAlO_x$ interlayer, after which the process transitions to a stable, ALD-like growth of Al_2O_3.[13]

3.5 Importance of the LiOH component

The above findings reveal a clear difference between the two plasma pretreatments. While TMA exposure on an Ar* pretreated surface leads to uncontrolled TMA decomposition, clear from the continuous growth and substantial Al and C uptake, the O_2^* pretreatment results in a more stable surface that supports ALD-like Al_2O_3 growth. The main compositional difference between these two surfaces is the presence of LiOH, which is only observed after O_2^* treatment. To determine whether this LiOH component indeed governs the surface reactivity towards TMA, rather than other plasma-related effects, an Ar* treated surface was dosed with 30 s H_2O at a pressure of 10^{-3} mbar, forming LiOH according to:

$$Li_2O + H_2O \rightarrow 2LiOH$$

This should result in a similar surface composition to that obtained after an O_2^* pretreatment (*i.e.* LiOH/Li_2O). As shown in Fig. 8, the Li_2O surface is indeed partially converted to LiOH after H_2O exposure, clear from the additional O 1s peak at 534 eV and the broadening of the Li 1s peak. When this surface is subsequently exposed to TMA, the resulting XPS spectra are very similar to TMA exposure after an O_2^* treatment. A self-limiting reaction occurs, with Al–CH_3, Li_2O and $LiAlO_x$ components observed at the surface.

Visually, the foil remained shiny without black spots and SEM imaging revealed no noticeable morphological changes (Fig. 9).

This additional result demonstrates that the presence of LiOH on the surface is critical for enabling ALD-like reactivity with TMA. Based on peak fitting of the O 1s signal, a LiOH : Li_2O ratio of approximately 30 : 70 is already sufficient to suppress TMA decomposition (Fig. S12). Analogous to surface Si–OH groups on a conventional Si wafer,[39] the LiOH groups act as

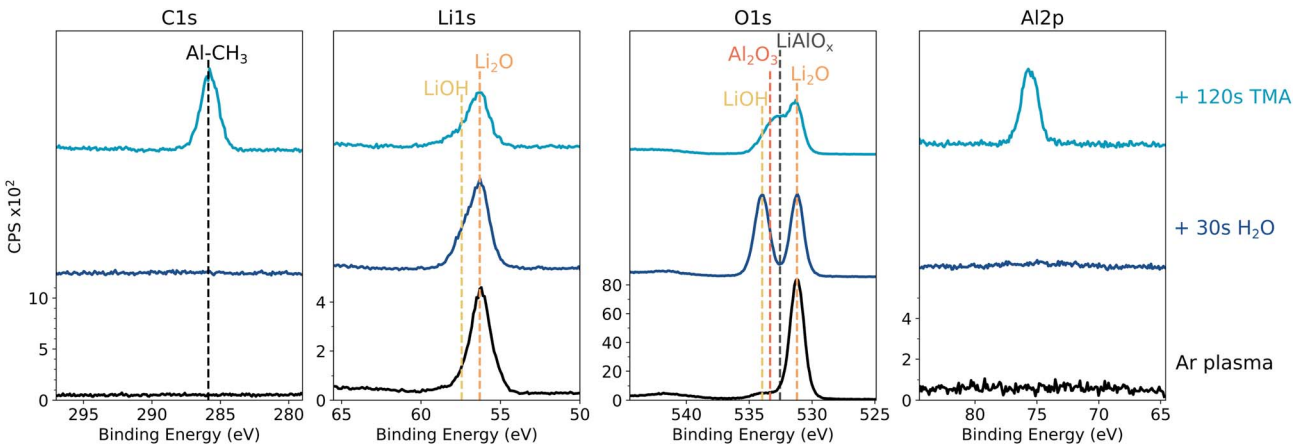

Fig. 8 (a) *In vacuo* XPS of an Ar* treated Li foil exposed to 30 s of H_2O and 120 s of TMA sequentially. Survey spectra can be found in Fig. S11.

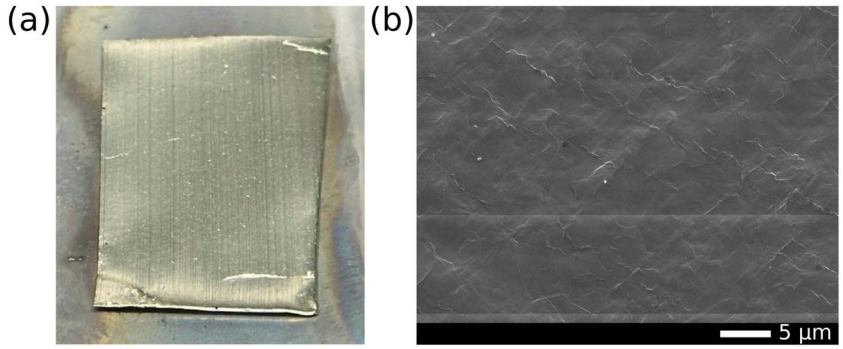

Fig. 9 (a) Visual and (b) SEM image of an Ar* treated Li foil exposed to 30 s of H_2O and 120 s of TMA sequentially.

Lewis bases that interact with the electron-deficient Al center of TMA. This results in a ligand exchange in which a proton from LiOH is transferred to a methyl group of TMA, releasing methane as a byproduct and forming (Li-)O–Al bonds.

Although H_2O dosing on an Ar*-treated lithium can lead to self-limiting reactions with TMA, the reaction of H_2O with metallic lithium itself is not self-limiting (Fig. S13). Continued reactions occur during H_2O exposure,[13,25] which makes reproducibility of the initial surface state more complicated. An O_2^* pretreatment is therefore able to provide a more controlled approach to obtain a LiOH surface and achieve subsequent ALD-like growth.

Using the Pilling–Bedworth ratios of the different components present at the surface after pretreatment, it is possible to explain the difference in reactivity towards the TMA precursor. Since LiOH and Li_2CO_3 exhibit PBR values of 1.26 and 1.35, respectively, it is expected that both materials are therefore able to form a continuous, passivating layer. On the contrary, the Li_2O surface layer has a lower PBR value of 0.57, which is consistent with the possibility that the layer contains potential cracks or voids at the nanoscale, resulting in uncontrolled TMA decomposition due to direct interaction between TMA and lithium. However, the formation of a LiOH-terminated surface by an O_2^* pretreatment makes self-limiting ALD-like growth possible.

Furthermore, this could clarify the discrepancy observed between our results and those reported by Kang *et al.*[20,23] for TMA exposure on as-received lithium foil. In our case, the native oxide layer was largely converted into Li_2CO_3, with only a minor Li_2O contribution remaining. Although not discussed by Kang *et al.*,[20,23] their lithium foil may have contained a higher fraction of unconverted Li_2O at the surface, thus exhibiting a different reactivity toward TMA.

4 Outlook

Although the main focus of this work is understanding how the lithium surface governs the initial TMA dosing, our findings have potential implications for the protection of reactive metal anodes.

Al_2O_3 coatings deposited by ALD have repeatedly been shown to improve cycling stability of lithium metal anodes.[11–13,19,22] However, in many cases, the initial lithium surface state was not controlled or explicitly reported. Since lithium plating and stripping are highly sensitive to the interfacial chemistry and its properties, variations in the initial surface state may contribute to differences in reported electrochemical performance. Our results imply that TMA exposure on as-received lithium can induce partial decomposition rather than homogeneous self-limiting reactions. When shorter precursor pulses, *i.e.* microdoses, are used, as done so in previous reports, decomposition may occur only locally and for a very short time, resulting in smaller nucleation sites. As a consequence, the decomposition is less obvious due to the minimal exposure time. This is supported by the results of Chen *et al.*,[13,23] where non-self-limiting microdoses of TMA on untreated lithium resulted in significantly higher uptake of deposited material compared to the eventual steady-state growth. As a result, continuous TMA-H_2O/O_2^* cycles may sustain growth at these sites or gradually cover them, eventually yielding an apparent uniform Al_2O_3 film, even though the initial growth mechanism deviated from ideal ALD behavior.

At the same time, previous work by Kang *et al.*[20,23] has shown that TMA decomposition forming a Li–Al–C layer can also result in promising cycling stability, provided the TMA exposure time is limited in extent. The improved cycling stability was attributed to the formation of a multilayered interphase with distinct chemical and structural properties. However, the observed decomposition behavior depended strongly on the freshness of the lithium surface, as the reaction was suppressed when a thicker native layer was present.

The present work demonstrates that the reaction pathway can be deliberately selected through plasma pretreatment. By employing O_2^*, self-limiting, layer-by-layer growth of (lithiated) Al_2O_3 can be achieved already from the first cycle. In contrast, Ar* pretreatment enables controlled removal of the native layer and reproducible initiation of the Li–Al–C formation. By providing well-defined starting surfaces and the ability to control the reaction pathway, the obtained results may lead to improved consistency of electrochemical performance and further optimization of protective coatings for highly reactive metal anodes.

5 Conclusion

In this work, a well-known ALD process, TMA and O_2 plasma, was directly deposited on metallic lithium and the growth mechanism was studied in detail for the first time. Deposition on as-received lithium, as commonly reported in ALD literature, was found to result in uncontrolled growth. The film thickness after 100 cycles not only exceeded that obtained during conventional ALD on SiO_2, but it was also not consistently reproduced. To obtain more control over the deposition, plasma pretreatments in vacuum were applied to establish well-defined and reproducible starting surfaces. After Ar plasma treatment, the native surface layer was completely removed, however, immediate formation of Li_2O is inevitable due to the extreme reactivity of lithium, even under UHV conditions. Subsequent exposure to TMA resulted in continuous precursor decomposition. After only 5 s of TMA dosing, the lithium foil became completely black and a thick Li–Al–C layer consisting of densely packed pillars was formed. After 30 s of exposure, the decomposition layer reached a thickness of approximately 2 μm. Based on the Pilling–Bedworth ratio for Li_2O, it is hypothesized that the oxide layer formed after Ar plasma is porous, thereby allowing the lithium underneath to react with incoming TMA and driving continuous growth. When O_2 plasma was used, a surface consisting of both LiOH and Li_2O was obtained. The foil remained smooth and shiny even after extended TMA exposure, indicating that a more ALD-like, self-limiting growth regime was achieved. The LiOH layer is proposed to moderate lithium's reactivity by providing well-defined sites for reaction with TMA. Self-limiting behavior was observed for TMA and O_2 plasma, although longer precursor dosing times were needed compared to saturation on SiO_2. Initial exposure resulted in the formation of a $LiAlO_x$ layer, but with increasing number of ALD cycles, a shift in XPS signal to (lithiated) Al_2O_3 was observed. Overall, the results presented in this work demonstrate that careful control of the initial lithium surface is essential for achieving reproducible ALD behavior. These findings underline the importance of critically considering the underlying reaction mechanisms, which differ greatly from these on conventional SiO_2 substrates. Reporting and standardizing starting surface conditions is strongly encouraged, as it has a significant influence on film growth and could facilitate future research in this field.

Conflicts of interest

There are no conflicts to declare.

Data availability

All data needed for interpretation of this work is available in the manuscript and supplementary information (SI). Supplementary information: XPS spectra showing the influence of pressure; XPS survey spectra of the initial surface states; Angle-resolved XPS spectra for as-received, Ar* and O_2* treated lithium foil; EDX spectra of TMA exposure on as-received lithium foil; XPS survey spectra of TMA exposure on Ar* treated lithium foil at different temperatures; EDX linescan of TMA exposure on Ar* treated lithium foil; XPS spectra of saturation behavior of TMA and O_2 plasma steps on O_2 plasma treated lithium foil; XPS survey spectra of TMA-O_2^* cycles on O_2^* treated Li and table with corresponding atomic percentages; SEM image of 100 TMA-O_2^* cycles on O_2^* treated surface; EDX spectra of 100 TMA-O_2^* cycles on O_2^* treated lithium compared to Si; XPS survey spectra of H_2O and TMA exposure on an Ar* treated lithium foil; XPS spectra of other controlled hydroxylation experiments; XPS spectra of different H_2O exposure times on Ar* treated lithium foil with corresponding survey spectra; Pilling–Bedworth ratio calculations. See DOI: https://doi.org/10.1039/d6ta00751a.

Acknowledgements

This work was supported by the GOA project from the Special Research Fund - UGent (01G02124) and VLAIO (Vlaams Agentschap Innoveren & Ondernemen) within the SBO project MESH-BAT (HBC.2023.0669). The authors acknowledge the financial support from Fonds Wetenschappelijk Onderzoek - Vlaanderen (FWO) for the FWO medium-sized research infrastructure project L-SCAN I003222N and for providing Tippi Verhelle with an SB grant (1SH9024N) and Lowie Henderick with a junior postdoctoral fellowship (1254324N). Siebe Coessens holds a grant (HBC.2022.0157) which is supported by VLAIO. Furthermore, a special thank you goes out to Geert Rampelberg and Stefaan Broekaert for their technical assistance and their eye for detail while developing/building the reactor used in this work and Olivier Janssens for his assistance during SEM operation.

References

1 J.-M. Tarascon and M. Armand, Issues and challenges facing rechargeable lithium batteries, *Nature*, 2001, **414**, 359–367.
2 J. Liu, *et al.*, Pathways for practical high-energy long-cycling lithium metal batteries, *Nat. Energy*, 2019, **4**, 180–186.
3 D. Aurbach, Review of selected electrode–solution interactions which determine the performance of Li and Li ion batteries, *J. Power Sources*, 2000, **89**, 206–218.
4 A. J. Sanchez and N. P. Dasgupta, Lithium Metal Anodes: Advancing our Mechanistic Understanding of Cycling Phenomena in Liquid and Solid Electrolytes, *J. Am. Chem. Soc.*, 2024, **146**, 4282–4300, PMID: 38335271.
5 Z. Han, C. Zhang, Q. Lin, Y. Zhang, Y. Deng, J. Han, D. Wu, F. Kang, Q.-H. Yang and W. Lv, A Protective Layer for Lithium Metal Anode: Why and How, *Small Methods*, 2021, **5**, 2001035.
6 Q. Wang, B. Liu, Y. Shen, J. Wu, Z. Zhao, C. Zhong and W. Hu, Confronting the Challenges in Lithium Anodes for Lithium Metal Batteries, *Advanced Science*, 2021, **8**, 2101111.
7 K. N. Wood, M. Noked and N. P. Dasgupta, Lithium Metal Anodes: Toward an Improved Understanding of Coupled Morphological, Electrochemical, and Mechanical Behavior, *ACS Energy Lett.*, 2017, **2**, 664–672.

8 A. J. Sanchez, E. Kazyak, Y. Chen, K.-H. Chen, E. R. Pattison and N. P. Dasgupta, Plan-View Operando Video Microscopy of Li Metal Anodes: Identifying the Coupled Relationships among Nucleation, Morphology, and Reversibility, *ACS Energy Lett.*, 2020, **5**, 994–1004.

9 K. N. Wood, E. Kazyak, A. F. Chadwick, K.-H. Chen, J.-G. Zhang, K. Thornton and N. P. Dasgupta, Dendrites and Pits: Untangling the Complex Behavior of Lithium Metal Anodes through Operando Video Microscopy, *ACS Cent. Sci.*, 2016, **2**, 790–801, PMID: 27924307.

10 K.-H. Chen, K. N. Wood, E. Kazyak, W. S. LePage, A. L. Davis, A. J. Sanchez and N. P. Dasgupta, Dead lithium: mass transport effects on voltage, capacity, and failure of lithium metal anodes, *J. Mater. Chem. A*, 2017, **5**, 11671–11681.

11 A. C. Kozen, C.-F. Lin, A. J. Pearse, M. A. Schroeder, X. Han, L. Hu, S.-B. Lee, G. W. Rubloff and M. Noked, Next-Generation Lithium Metal Anode Engineering *via* Atomic Layer Deposition, *ACS Nano*, 2015, **9**, 5884–5892, PMID: 25970127.

12 E. Kazyak, K. N. Wood and N. P. Dasgupta, Improved Cycle Life and Stability of Lithium Metal Anodes through Ultrathin Atomic Layer Deposition Surface Treatments, *Chem. Mater.*, 2015, **27**, 6457–6462.

13 L. Chen, J. G. Connell, A. Nie, Z. Huang, K. R. Zavadil, K. C. Klavetter, Y. Yuan, S. Sharifi-Asl, R. Shahbazian-Yassar, J. A. Libera, A. U. Mane and J. W. Elam, Lithium metal protected by atomic layer deposition metal oxide for high performance anodes, *J. Mater. Chem. A*, 2017, **5**, 12297–12309.

14 Y. Cao, X. Meng and J. W. Elam, Atomic Layer Deposition of Li_xAl_yS Solid-State Electrolytes for Stabilizing Lithium-Metal Anodes, *ChemElectroChem*, 2016, **3**, 858–863.

15 C.-F. Lin, A. C. Kozen, M. Noked, C. Liu and G. W. Rubloff, ALD Protection of Li-Metal Anode Surfaces – Quantifying and Preventing Chemical and Electrochemical Corrosion in Organic Solvent, *Adv. Mater. Interfaces*, 2016, **3**, 1600426.

16 L. Chen, K.-S. Chen, X. Chen, G. Ramirez, Z. Huang, N. R. Geise, H.-G. Steinrück, B. L. Fisher, R. Shahbazian-Yassar, M. F. Toney, M. C. Hersam and J. W. Elam, Novel ALD Chemistry Enabled Low-Temperature Synthesis of Lithium Fluoride Coatings for Durable Lithium Anodes, *ACS Appl. Mater. Interfaces*, 2018, **10**, 26972–26981, PMID: 29986134.

17 P. K. Alaboina, S. Rodrigues, M. Rottmayer and S.-J. Cho, In Situ Dendrite Suppression Study of Nanolayer Encapsulated Li Metal Enabled by Zirconia Atomic Layer Deposition, *ACS Appl. Mater. Interfaces*, 2018, **10**, 32801–32808, PMID: 30157373.

18 M. Wang, X. Cheng, T. Cao, J. Niu, R. Wu, X. Liu and Y. Zhang, Constructing ultrathin TiO_2 protection layers *via* atomic layer deposition for stable lithium metal anode cycling, *J. Alloys Compd.*, 2021, **865**, 158748.

19 E. Jin, K. Tantratian, C. Zhao, A. Codirenzi, L. V. Goncharova, C. Wang, F. Yang, Y. Wang, P. Pirayesh, J. Guo, L. Chen, X. Sun and Y. Zhao, Ionic Conductive and Highly-Stable Interface for Alkali Metal Anodes, *Small*, 2022, **18**, 2203045.

20 D. Kang, J. W. Elam and A. U. Mane, Formation of lithium-metal-carbon protecting layer and removal of lithium carbonate on lithium metal, *US Patent*, 2022.

21 B. Zhao, J. Li, M. Guillaume, V. Cremers, L. Henderick, J. Dendooven and C. Detavernier, Atomic layer deposition of yttrium oxide as a protective coating for lithium metal anodes, *Dalton Trans.*, 2023, **52**, 7302–7310.

22 S. Pakseresht, V. Miikkulainen, F. A. Obrezkov, A. W. M. Al-Ogaili, J. Lahtinen and T. Kallio, Atomic layer deposition for protecting lithium metal anodes to high-voltage battery applications, *J. Power Sources*, 2025, **653**, 237731.

23 K. Park, Y. L. Kim, J. G. Connell, C. Liu, H. Kim, S. Kim, C. T. Nguyen, A. U. Mane, D. Kang and J. W. Elam, Chemical Vapor Transformation of Lithium Metal: Mechanism and Enhanced Stability, *ACS Appl. Mater. Interfaces*, 2025, **17**, 67763–67775, PMID: 41342298.

24 S.-K. Otto, Y. Moryson, T. Krauskopf, K. Peppler, J. Sann, J. Janek and A. Henss, In-Depth Characterization of Lithium-Metal Surfaces with XPS and ToF-SIMS: Toward Better Understanding of the Passivation Layer, *Chem. Mater.*, 2021, **33**, 859–867.

25 S.-K. Otto, T. Fuchs, Y. Moryson, C. Lerch, B. Mogwitz, J. Sann, J. Janek and A. Henss, Storage of Lithium Metal: The Role of the Native Passivation Layer for the Anode Interface Resistance in Solid State Batteries, *ACS Appl. Energy Mater.*, 2021, **4**, 12798–12807.

26 N. Fairley, V. Fernandez, M. Richard-Plouet, C. Guillot-Deudon, J. Walton, E. Smith, D. Flahaut, M. Greiner, M. Biesinger, S. Tougaard, D. Morgan and J. Baltrusaitis, Systematic and collaborative approach to problem solving using X-ray photoelectron spectroscopy, *Appl. Surf. Sci. Adv.*, 2021, **5**, 100112.

27 K. N. Wood and G. Teeter, XPS on Li-Battery-Related Compounds: Analysis of Inorganic SEI Phases and a Methodology for Charge Correction, *ACS Appl. Energy Mater.*, 2018, **1**, 4493–4504.

28 JEOL Environmental Airlock system. https://www.jeolusa.com/RESOURCES/Electron-Optics/Documents-Downloads/environmental-airlock-for-jsm-it210-series-sem.

29 U. Wietelmann, Surface-passivated lithium metal and method for the production thereof, *US Pat.*, 2013.

30 B. Zhao, J. Li, M. Guillaume, J. Dendooven and C. Detavernier, In vacuo XPS investigation of surface engineering for lithium metal anodes with plasma treatment, *J. Energy Chem.*, 2022, **66**, 295–305.

31 F. She, A. Gao, P. Jiang, Y. Zhou, X. Zhang, M. Yang, L. Gong, J. Chen, X. Lu and F. Xie, Exploring the stability of lithium metal surface by X-ray photoelectron spectroscopy, *Vacuum*, 2023, **211**, 111893.

32 V. R. Rai, V. Vandalon and S. Agarwal, Surface Reaction Mechanisms during Ozone and Oxygen Plasma Assisted Atomic Layer Deposition of Aluminum Oxide, *Langmuir*, 2010, **26**, 13732–13735, PMID: 20806961.

33 N. Hornsveld, W. Kessels and M. Creatore, Mass Spectrometry Study of Li_2CO_3 Film Growth by Thermal and Plasma-Assisted Atomic Layer Deposition, *J. Phys. Chem. C*, 2019, **123**, 4109–4115.

34 H.-E. Nieminen, M. Chundak, M. J. Heikkilä, P. R. Kärkkäinen, M. Vehkamäki, M. Putkonen and M. Ritala, In vacuo cluster tool for studying reaction mechanisms in atomic layer deposition and atomic layer etching processes, *J. Vac. Sci. Technol., A*, 2023, **41**, 022401.
35 C. Hinnen, D. Imbert, J. Siffre and P. Marcus, An *in situ* XPS study of sputter-deposited aluminium thin films on graphite, *Appl. Surf. Sci.*, 1994, **78**, 219–231.
36 N. Pilling, The oxidation of metals at high temperature, *J. Inst. Met.*, 1923, **29**, 529–582.
37 Y. Qi, J. Liu, M. Feng, K. Tantratian, L. Chen, X. Xiao and A. K. Sachdev, From the Passivation Layer on Aluminum to Lithium Anode in Batteries, *Metall. Mater. Trans. A*, 2025, **56**, 429–438.
38 O. Renault, L. G. Gosset, D. Rouchon and A. Ermolieff, Angle-resolved x-ray photoelectron spectroscopy of ultrathin Al_2O_3 films grown by atomic layer deposition, *J. Vac. Sci. Technol., A*, 2002, **20**, 1867–1876.
39 R. L. Puurunen, Surface chemistry of atomic layer deposition: A case study for the trimethylaluminum/water process, *J. Appl. Phys.*, 2005, **97**, 121301.